Int. J. New. Chem., 2023, Vol. 10, Issue 3, pp. 197-212.

International Journal of New Chemistry

Published online 2023 in http://www.ijnc.ir/.

Open Access

Print ISSN: 2645-7236

Online ISSN: 2383-188x

Original Research Paper

Theoretical study of some graphene-Like nanoparticles as the anodes in K−ion Batteries

Fatemeh Mohammad Alipour[1], Mirzaagha Babazadeh[1],* , Esmail Vessally[2],*, Akram Hosseinian [3], Parvaneh Dalir Kheirollahi Nezhad [2]

*[1]*Department of Chemistry, Tabriz Branch, Islamic Azad University, Tabriz, Iran*

[2]Department of Chemistry, Payame Noor University, Tehran, Iran

[3]School of Engineering Science,College of Engineering, University of Tehran, Tehran, Iran

Received: 2023-02-01 ***Accepted: 2023-05-25*** ***Published: 2023-06-01***

ABSTRACT

In this research, density functional theory (DFT) calculations were carried out for investigating the adsorption of the K atom and ion on the surface of three sheet-like nanoparticles, namely nanosheet, corannulene (CRN) and sumanene (SMN). Density of states (DOS) diagrams, geometry optimizations and total energies were all studied using the M06−2X level of theory with the basis set 6−31+G (d, p). The Ead for SMN-i was found to be more negative, which increased in the following order: SMN-i > nano-sheet > CRN-i > CRN > SMN. The main goal of this work was to compute the cell voltage (Vcell) for K−ion batteries (KIBs). Here, the Vcell for SMN was the highest value, which increased in the following order: SMN > CRN > nano-sheet > SMN-i > CRN-i. The current study provided a theoretical description and promising candidate of the above mentioned nano-structures as anode materials in KIBs ion batteries.

Keywords: DFT calculations; nanoparticles; sheet-Like nanoparticles;cell voltage

Introduction

Owing to the increasing demand for electronic devices, especially electric vehicles, the expansion of the market lithium-ion batteries (LIBs) is predicted over the next ten years [1]. However, the two important elements used in LIBs, including cobalt (Co) and lithium (Li), are

geographically located on earth, making their supply difficult due to price volatility [2]. Moreover, due to the fact that Co and Li are abundant, there have been growing concerns for their long-term sustainability. The current Li and Co resources in the world have been estimated to be 80 and 20 million tons21% and 28% of which are economically extractable, respectively [3]. Most of Co resources are found in the Democratic Republic of the Congo, where there have been reports about human rights abuses related to its mining [4,5]. Hence, it is necessary to develop alternative high-performance battery as good as LIBs. An alternative can be development of sodium- and potassium-ion batteries (KIBs and NIBs).

The price of N and K carbonate (ton= 1$200 and $1000 respectively) is significantly lower than Li carbonate ($ 8,750) [6-8]. Moreover, in the processes of manufacturing LIBs over the pasty thirty years, NIBs as well as KIBs can be employed as the anodes Batteries [9]. The storage and transportation of both NIBs and KIBs in their fully discharged state is implied by their replacement with Cu, which improves safety and significantly reduces the costs of transportation and storage [6].

Nevertheless, one of the important advantages of KIBs over NIBS is the intercalation of K ions into the graphite electrodes which are employed in LIBs [10,1]. Recently, numerous reports have been published on such materials [6,8,12–16]. Accordingly, an analysis and general overview of the most encouraging KIB electrolytes and electrode materials are provided here. Our focus is particularly on the KIB with high performance which are capable of replacing the LIBs. Moreover, a brief techno-economic analysis of KIBs in comparison NIBs and LIBs is presented for applications. Within this study, we compared the cell voltage (V_{cell}) of three nano-structures, namely nanosheet, corannulene (CRN) and sumanene (SMN), based on Na−ion battery (Table 1). The results of this computational study are expected to assist experimental chemists in improving the NIB equipment.

Computational details

We calculated the natural bond orbitals (NBO) of the complex of K^+/K−nano-structure the hybridization and charge study. We calculated the adsorption energy of K and K+ as follows:

$$E_{ad} = E_{complex} - E_{nano\text{-}structure} - E_{K/K+} + E_{BSSE} \quad (1)$$

where, $E_{nano\text{-}structure}$ is the energy of the nano-structures. $E_{complex}$ is the energy of each nano-structure, on the surface of which K or K^+ was adsorbed.

EBSSE signifies the basis set superposition error which was computed using the counterpoise method [19].

The energy of the HOMO−LUMO gap (Eg) was computed as follows:

$E_g = E_{LUMO} - E_{HOMO}$ (2)

where E_{LUMO} is the energy of the HOMO level and E_{HOMO} is that of the LUMO level.

The change in E_g was calculated as follows:

$\Delta E_g = [(E_{g2} - E_{g1})/E_{g1}] * 100$ (3)

where, E_{g1} and E_{g2} signify the nano-structures value and the complex value. This parameter indicates the electronic sensitivity of the nano-structures to the adsorption of K/K^+. The Gaussum software program was utilized for computing the plots of DOS [20].

3. Results and discussions

The corannulene (CRN), sumanene (SMN) and nano-sheet have the formulas $C_{21}H_{12}$, $C_{20}H_{10}$, and $C_{54}H_{18}$, respectively. We used the hydrogen atoms for capping the nano-structures boundary carbon atoms. We designated the nano-structures to see how they interact with K and K+. Later, we computed and discussed V_{cell} of the complexes. All the regions at top of hexagon or pentagon ring was checked.

3.1 Adsorption of K/K^+ onto the sumanene (SMN)

The SMN is a bowl-shaped molecule and its bowl depth is118 picometers which is equivalent to 1.18 angstrom and its six hub C atoms are pyramidalized by 9°, demonstrating significant bond alternation from 1.38 to 1.43 angstrom and there is a benzene ring in its core and its periphery with cyclopentadiene as well (see Figure 1) [21-26].

For the possible interaction with K and K^+. The middle top of hexagon or pentagon rings where there was K or K^+ was the place where we found the global minima for all complexes.

In the conclave surface, the interaction of K^+ with SMN was more (-37.66 kcalmol^{-1}) compared to their interaction in the convex surface. Also, the interaction of K^+ with CRN in the concave surface was slightly more (-0.95 kcalmol^{-1}) compared to their interaction in the convex surface

The position of adsorption is considered important in the comparison of computed datra on both convex and concave surfaces

The energy of the HOMO was −6.95 eV and that of the LUMO was −0.29 eV. Hence, E_g The energy of the HOMO was −6.95 eV and that of the LUMO was −0.29 eV. Hence, E_g was 6.67 eV (Table 1). All possible interactions between K+/K and both outside or inside the bowl had to be investigated for the adsorption behavior of K+/K onto SMN.

Figure 3 shows the %ΔEg to the lower energies for the SMN−K^+ complex. The HOMO and LUMO levels stabilized by K^+ adsorption on SMN at the most optimal point is sharp for LUMO level. There was a major stabilization in the LUMO from −0.29 eV in SMN to −4.62 eV in the complex of SMN−K^+ (Table 1), cause to is slightly diminish in the Eg. The variations in HOMO, LUMO and Eg values are demonstrated in Figure 3 through DOS plots.

The partial DOS (PDOS) demonstrated the creation of a new level at E_g gap of pristine which arose from K^+ cation; and there was a negligible decrease in E_g of the complex of K^+−SMN complex (Figure 4).

The impact of atomic K adsorption onto the electronic properties of SMN−K was not similar to that of SMN−K^+. Different to the K^+ adsorption, the K adsorption mainly leads the SOMO unstable because of being an unpaired electron in HOMO of the SMN−K complex. The value of the SOMO level is shifted from −6.95 to −3.53 eV which is slightly occupied. In consistent to the keen energy shift, the shape of HOMO is shifted mainly through transfer to the adsorbing zone. In Table 1 and Figure 4 the energy value of the LUMO level is slightly shifted from −0.29 to −0.52 eV. The E_g value is considerably narrowed by about 54.87%, demonstrating that the effect of K adsorption on the E_g is much more than that of the K^+ adsorption. The PDOS in Figure 4 obviously demonstrates the formation of a new level Eg gap of pristine which arose from the atomic K, causing a decrease in E_g of the complex of K−SMN.

From the analysis of PDOS plot of K^+− SMN and K− SMN, the electronic charge transfer elucidated that a new level was formed from K^+ at the LUMO area leads to diminish in E_g. In the K−SMN complex, the interaction of K atom onto SMN leads to an instable SOMO.

that results in an increase in the electronic charge transport. The electronic charge transfer for the complex of K−SMN was more compared to that of the complex of K^+−SMN since E_g for the former complex was less than that of latter complex.

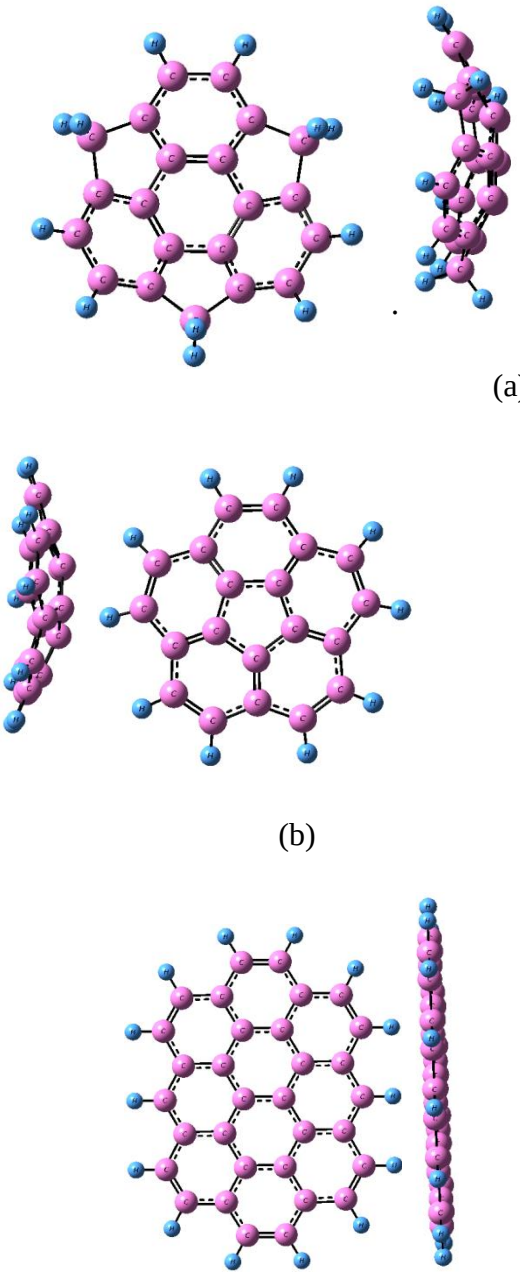

(a)

(b)

(c)

(a)**Figure 1.** The optimized molecular structure of (a) SMN; (b) CRN; (c) nano-sheet

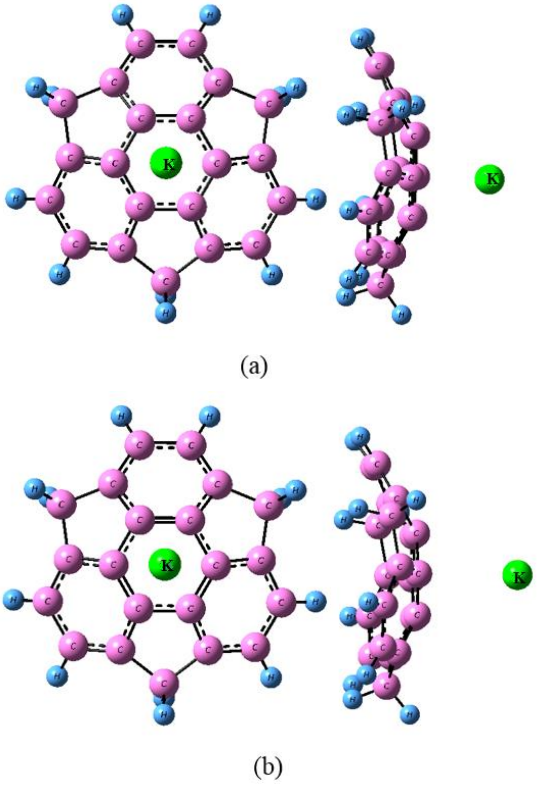

(a)

(b)

Figure 2. Optimized structures of K^+ and K−SMN complexes. (a) K^+−SMN complex (b) K−SMN complex. Pink, green and blue balls are carbon, sodium and hydrogen atoms.

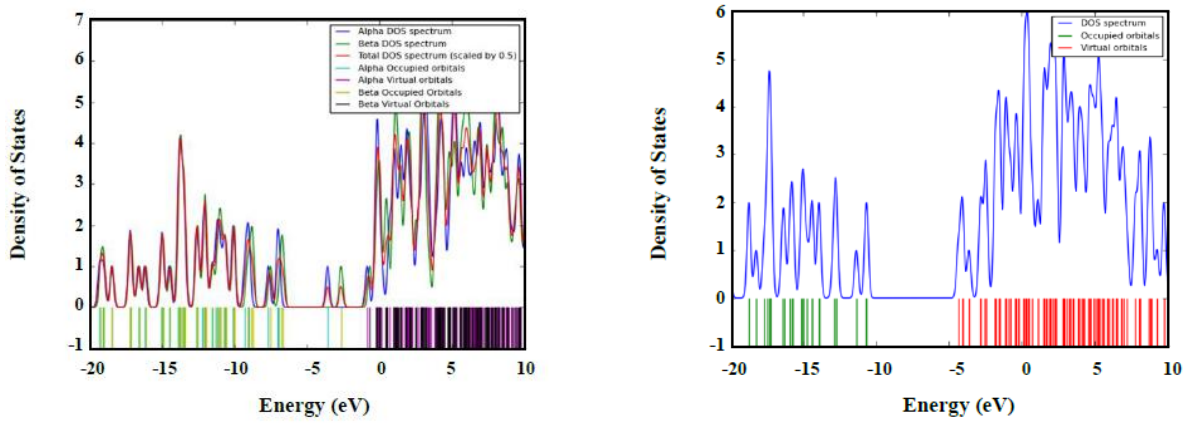

Figure 3. DOS plots of SMN (right) and complex of K^{+}− SMN (left).

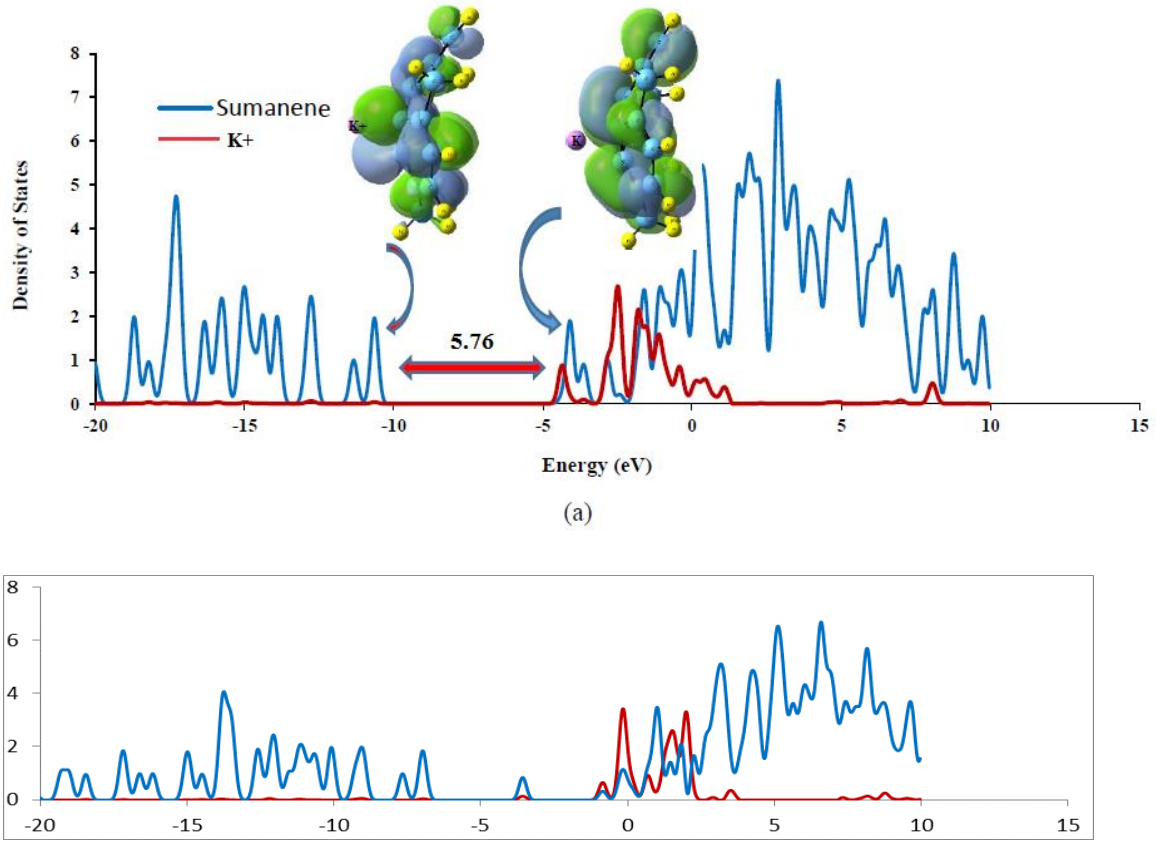

Figure 4. PDOS plots of K^{+}− SMN and K− SMN. (a) PDOS plot of K^{+}− SMN (b) PDOS plot of K− SMN

Adsorption of K/K$^+$ inside the bowl of sumanene

Figure 5 shows the optimized structures the K^+ and K inside the 6−membered rings plane of SMN-i with lengths of 1.65 and 2.51 Å from carbon atom, respectively. This demonstrates a good interaction between SMN-i and both K^+ ion and atomic K. Table 1 illustrates the adsorption energy, E_{ad}, of the K^+ inside the SMN-i is −37.66 kcal mol^{-1} which was larger than that of the atomic K (−14.30 kcal mol^{-1}). These adsorption energies, E_{ad}, expression an appropriate interaction between SMN and K^+ ion as well as K atom inside the bowl of SMN-i with respect to outside the bowl of SMN.

The %ΔEg to the lower energies for K/K$^+$ inside the bowl of SMN-i was similar to outside the bowl of SMN; stabilizing during K^+ adsorption over SMN which the stabilization is sharp for LUMO level. There was a major stabilization in the LUMO level from −0.29 eV in SMN-i to −4.64 eV in the complex of K^+−SMN-i (Table 1). The DOS plots represent the changes in HOMO, LUMO and E_g in Figure 6.

The K adsorption mainly makes the SOMO instable because of an unpaired electron in the HOMO of the complex of K−SMN-i. This SOMO level causes to diminished from −6.95 to −3.61 eV that was relatively occupied. As shown in Figure 6 and Table 1, the energy of the LUMO level is slightly augmented from −0.29 to −0.54 eV. As a consequence of great change in HOMO, the Eg is remarkably narrowed by about 53.97%, representing that the effect of K adsorption on the E_g is much more than that of the K^+ adsorption process

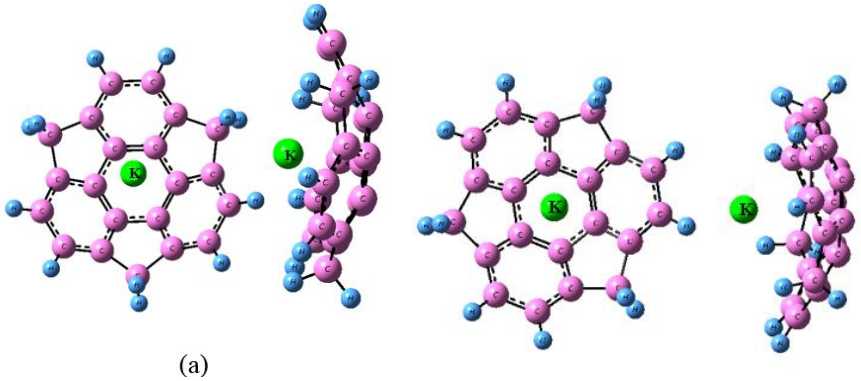

(a)

Figure 5. The optimized structure of K^+ and complex of K−SMN-i. (a) complex of K^+−SMN-i (b) complex of K−SMN-i. Blue, green, and pink balls are hydrogen, sodium and carbon atoms

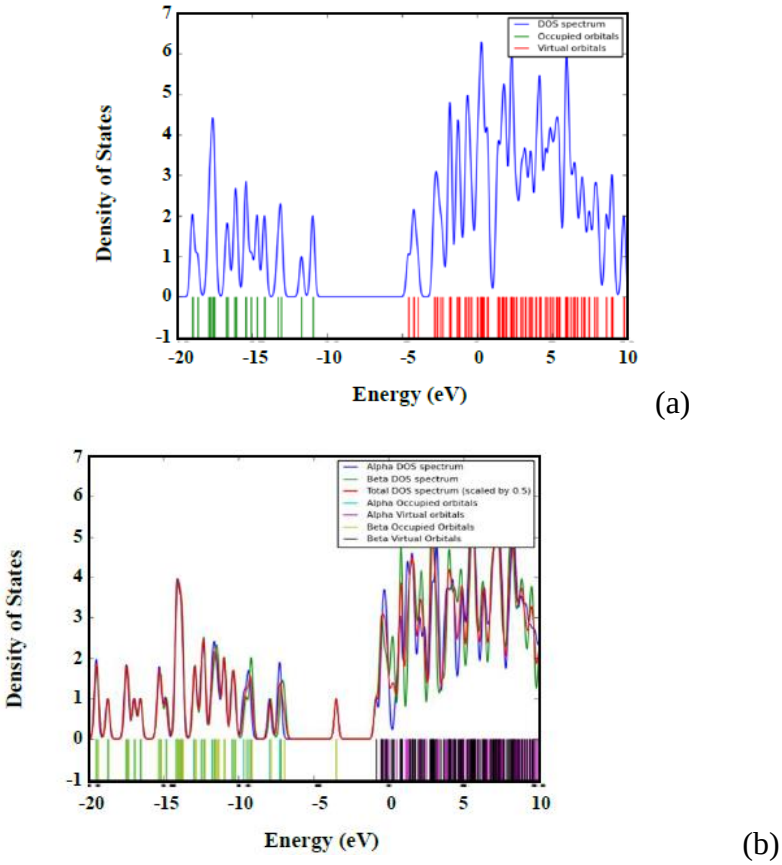

Figure 6. Density of states (DOS) plot of (a) K^+− SMN-I; (b) K−SMN-i.

Adsorption of K/K^+ outside the bowl of corannulene

The CRN molecules consists of a cyclopentane ring that is fused with 4 benzene rings knows as a buck bowl. With a barrier energy of 10.2 kcal/mol at −64 °C, the CRN nano-structure has a bowl−to−bowl inversion [54]. Figure 7 shows that ionic and atomic K occurred above the 5−membered ring's plane of CRN with distances of 1.58 and 2.07 Å from C atom, respectively. As shown in Table 1, E_{ad}, of K^+ onto CRN was −35.73 kcal mol^{-1}, which was higher compared to that of K (−7.52 kcal mol^{-1}). The interactions between CRN and both K^+ and K were stronger compared to those of surname. The $\%\Delta E_g$ to the lower energies (more negative) for the CRN−K^+ complex (Fig. 8) which shifting is sharp for LUMO level. The LUMO level considerably stabilized from −1.14 eV in CRN to −4.66 eV in the CRN−K^+ complex (Table 1), leading to slightly diminish in the E_g (∼−3.27%)

The changes in HOMO, LUMO and E_g were shown in Figure 8 through DOS plots. DOS plots demonstrated the formation of a new peak at E_g gap of pristine that arose from K^+, leading to negligible decrease in the E_g of the complex of K^+−CRN (Figure 8). The adsorption of K on CRN caused the SOMO to be instable due to an unpaired electron in HOMO of the complex of CRN−K. There was a change in the SOMO level from −7.56 for CRN to −3.55 eV for the complex of CRN−K that was singly occupied. By transferring to the adsorbing region, there was considerable change in the shape of HOMO. There was no change in energy of the LUMO level as illustrated in Figure 8 and Table 1. The E_g is significantly diminished by 69.47%, indicating that the K adsorption changes the E_g much more than that of the K^+ adsorption. The changes in HOMO, LUMO and E_g are demonstrated in Figure 8 using density of state (DOS) diagrams

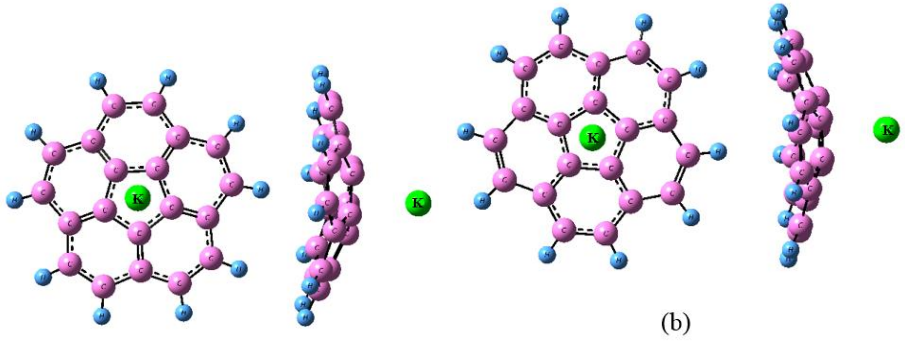

Figure 7. Optimized structures of K^+ and K−CRN complexes. (a) K^+−CRN complex (b) K−CRN complex, Distances are in Å. Pink, green and blue balls are carbon, sodium and hydrogen atoms.

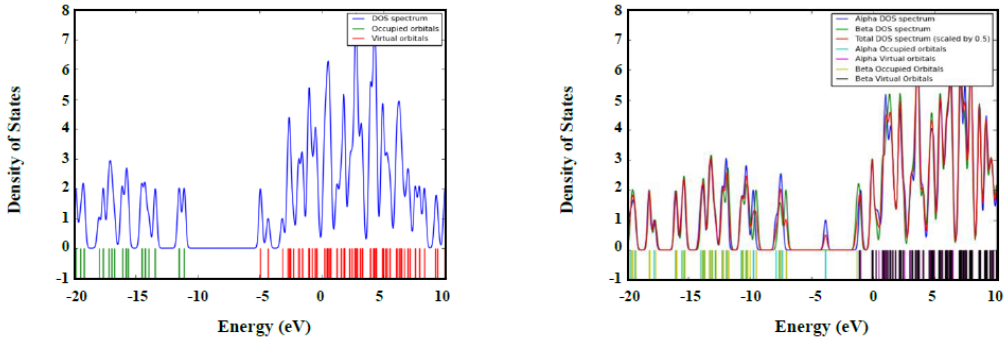

Figure 8. Density of states (DOS) plot of (a) K^+− CRN; (b) K−CRN.

Adsorption of K/K$^+$ inside the bowl of corannulene (CRN)

Figure 9 shows the optimized structures of the K^+ ion and K atom inside the plane of the five−membered ring of CRN with distances of 1.64 and 2.14 Å, respectively. In Table 1 observed the adsorption energy, E_{ad}, of the K^+ ion inside the CRN is −36.68 kcal mol^{-1} that was higher than that of the K neutral (−15.74 kcal mol^{-1}).

The ΔE_g levels and E_g for K/K$^+$ inside the bowl of CRN is more or less similar to outside the bowl of CRN. The LUMO level considerably stabilized from −1.14 eV in CRN to −4.85 eV in the K^+−CRN−i complex (Table 1); causing to slightly diminish in the E_g (∼−1.09%). Figure 10 demonstrates the changes in HOMO, LUMO and E_g through DOS plots. This SOMO level is changed from −7.56 for CRN to −3.76 eV for K−CRN−i complex that was singly occupied. AS shown in Table 1 and Figure 10, there was a slight change in the energy of the LUMO level from −1.14 to −1.44 eV. Due to the large change in the HOMO, E_g reduced by approximately −63.86%, indicating that the effect of K adsorption on the E_g is much more than that of the K^+ adsorption process.

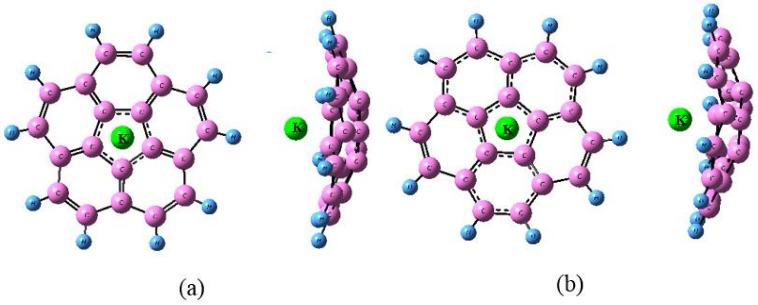

Figure 9. Optimized structures of K^+ and K−CRN−i complexes. (a) K^+−CRN-i complex (b) K−CRN-i complex. Pink, green and blue balls are carbon, sodium and hydrogen atoms.

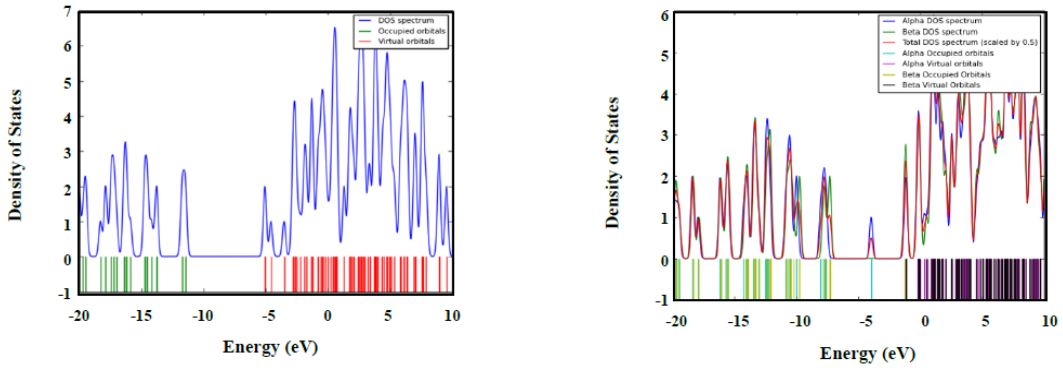

Figure 10. Density of states (DOS) plot of (a) K^+− CRN-i; (b) K−CRN-i.

Adsorption of K/K^+ over nanosheet

A nanosheet is a two-dimensional nano-structure with thickness in a scale ranging from 1 to 100 nm [1]. Figure 11 shows the optimized structures of the K^+ ion and K atom above the plane of the six−membered ring of nanosheet with distances of 1.52 and 2.02 Å, respectively (Fig. 11). The adsorption energy, E_{ad}, of K^+ on the nanosheet is −32.83 kcal mol^{-1} that is larger than that of the K neutral (−9.76 kcal mol^{-1}) (Table 1).

Figure 12 shows the ΔE_g levels for the nanosheet−K^+ complex. The LUMO level mainly stabilized from −1.59 eV in nanosheet to −4.71 eV in the nanosheet−K^+ complex (Table 1), which causes a slight decrease in E_g (∼−3.9%). Figure 12 demonstrates the changes in HOMO, LUMO and Eg through DOS plots. The K adsorption mainly causes the SOMO demonstrates the changes in HOMO, LUMO and E_g through DOS plots. It was very interesting that distance of K from CRN plane was SMN smaller than that of K^+ while distance of K from SMN plane was larger than that of K^+. It seemed that the 6-membered ring in SMN was aromatic in which there was a strong cation interaction that led to diminish distance of K^+ and SMN plane, while the 5-membered ring in CRN was not aromatic and the C atoms of 5-membered ring had slightly positive charge which leads to larger distance between K^+ and CRN plane

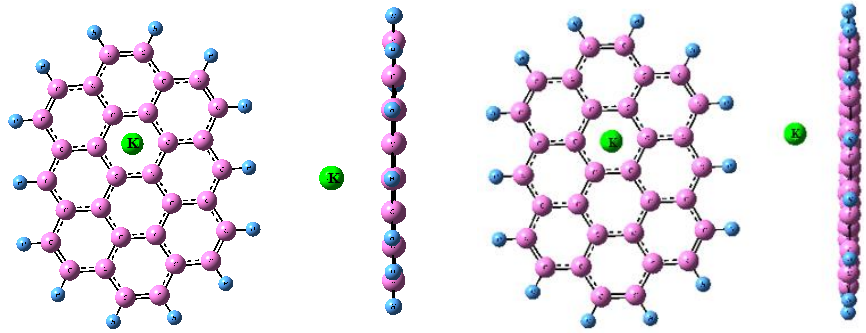

Figure 11. Optimized structures of K^+ and K−Sheet complexes. (a) K^+−Sheet complex (b) K−Sheet complex, Distances are in Å. Pink, green and blue balls are carbon, sodium and hydrogen atoms.

Comparison the nano-structures in the K^+−ion batteries (KIBs)

Three kinds of nano-structures were proposed as anodes for NIBs. The process of typical reactions in the cathode and anode is as follows [53]:

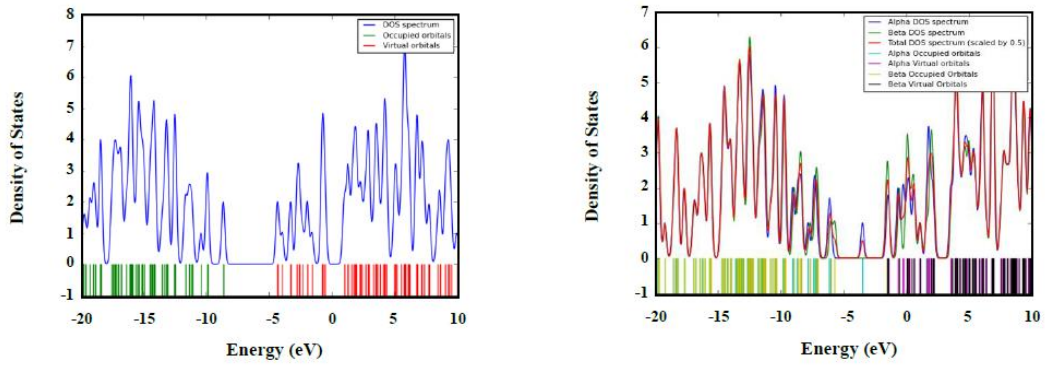

(a) **(b)**

Figure 12. Density of states (DOS) plot of (a) K^+− Sheet; (b) K−Sheet

Anode: K−nanostructure ↔ K^+− nano-structure + e^- (4)

This reaction can be divided into several reactions that are presented below:

Cathode: $K^+ + e^- \leftrightarrow K$ (5)

The ΔG_{cell} signifies the Gibbs free energy difference of the total between K atom and nano-structure obtain more negative and higher ΔE_{cell}. In conclusion, the strong adsorption of K^+ and weak adsorption of K on the nano-structure resulted in high V_{cell} (Table 1). The adsorption energy between K^+ and nano-structures, E_{ad}, is increased in the order: SMN-i > nano-sheet > CRN-i > CRN > SMN. The ΔE_{cell}, and V_{cell} are calculated for three nano-structures which were provided in Table 1 and depicted in Figure 13. The ΔE_{cell}, and V_{cell} values for three nano-structures in NIBs changed in the same order: SMN > CRN > nano-sheet > SMN-i > CRN-i. The largest ΔE_{cell} and V_{cell} values of −27.74 kcal mol and 1.20 V, respectively, belong to SMN. The V_{cell} for SMN is the highest because the interaction between SMN and the K neutral is the lowest. The strong interaction between K^+ and nano-structure and the weak interaction between the K atom and nano-structure led to high amount of V_{cell} for NIBs−nano-structure. The ΔE_{cell}

and V_{cell} resulted in high cell voltage. The amount of entropy and volume contribution to V_{cell} was assumed to be negligible (< 0.01 V) in previous reports.

Therefore, the V_{cell} for K^+– or K–nano-structure can be determined by calculating the internal energy change (ΔE) from Equations 6 and 8 as follows:

$$\Delta E_{cell} \sim \Delta G_{cell} = E_K + E_{K+-Knostructure} - E_{K^+} - E_{K-nano-structure} \quad (9)$$

Equation 9 indicates that the strong interaction between K^+ and nano-structure and weak NIBs−nanosheet were −22.92 kcal/mol and 0.99 V, respectively, which are lower than the values of SMN. The lowest V_{cell} value belonged to the NIBs−CRN−i because of the highest interaction between the K neutral and CRN−i. In general, the V_{cell} value for NIBs−nano-structures are from −0.88 to −1.20 V, makes these nano-structures the promising candidates that can be employed for manufacturing anodes for NIBs. We can assert that the interaction between the K neutral and nano-structures plays an important role in V_{cell} with respect to the interaction between the K^+ neutral and nano-structures

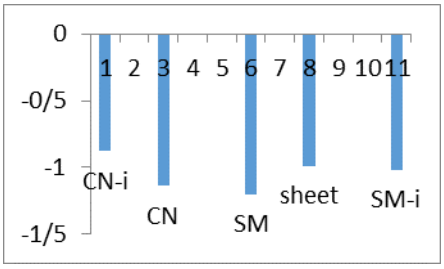

Figure 13. The V_{cell} diagram *vs.* different nano-structures as an anode of K ion batteries, NIBs.

4. Conclusions

Within this study, we scrutinized adsorption of K^+ and K onto the surface of three nano-structures, namely nano-sheet, SMN, and CRN for finding a suitable anode for NIBs. There was stronger interaction between the surface of above-mentioned nano-structures and K^+ in comparison with K, which demonstrates that these nano-structures are suitable anodes for NIBs. E_{ad} between the nano-sheet and K^+ was the highest, which was in the following order: SMN-i > nano-sheet > CRN-i > CRN > SMN. Nevertheless, V_{cell} was the highest for SMN, which was in

the following order: SMN > CRN > nano-sheet > SMN-i > CRN-i. A key factor determining V_{cell} is the interaction of nano-structures with K+ and K. The weak and strong interaction of nano-structures with K and K^+, respectively, results in a high V_{cell}.

References

[1] Xu W., Wang J., Ding F., Chen X., Lisybulin E., Zhang Y. and Zhang J.−G., Scale-up production of high-tap-density carbon/MnOx/carbon nanotube microcomposites for Li-ion batteries with ultrahigh volumetric capacity, *Energy Environ. Sci*., **7**, 513–537 (2014).

[2] Er D., Li J., Liguib M., Gogotsi Y., Shenoy V.B., Ti_3C_2 MXene as a High Capacity Electrode Material for Metal (Li, Na, K, Ca) Ion Batteries, ACS Appl. Mater Interfaces **6**,11173–11179 (2014).

[3] Siadati S.A., Vessally E., Hosseinian A., Edjlali L., Possibility of sensing, adsorbing, and destructing the Tabun-2D-skeletal (Tabun nerve agent) by C20 fullerene and its boron and nitrogen doped derivatives, *Synthetic Met*. **220**, 606–611(2016).

[4] Siadati S.A., Vessally E., Hosseinian A., Edjlali L., Determining the status of activity of daily living (ADL) and instrumental activity of daily living (IADL) in healthy and cognitive impaired elderlies, *Talanta* **162**, 505–510 (2017).

[5] Vessally E., Soleimani–Amiri S., Hosseinian A., Edjlal L., Bekhradnia A., Selective detection of cyanogen halides by BN nanocluster: a DFT study, *Physica E* , **87**, 308–311 (2017).

[6] Hosseinian A., Saedi Khosroshahi E., Nejati K., Edjlali E., Vessally E., A DFT study on graphene, SiC, BN, and AlN nanosheets as anodes in Na-ion batteries, *J. Mol. Model*. **23**,354 (2017).

[7] Nejati K., Hosseinian A., Edjlali L., Vessally E., The effect of structural curvature on the cell voltage of BN nanotube based Na-ion batteries, *J. Mol. Liq*. **229**, 167–171(2017).

[8] Subalakshmi P., Sivashanmugam A., CuO nano hexagons, an efficient energy storage material for Li-ion battery application, *J. Alloys Compd.* **690**, 523–531(2017).

[9] Nejati K., Hosseinian A., Bekhradnia A., Vessally E., L.Edjlal, Na-ion batteries based on the inorganic BN nanocluster anodes: DFT studies, *J Mol Graph Model*, **74**, 1–7(2017).

[10] Jing Y., Zhou Z., Cabrera C.R., Chen Z.F., Graphene, inorganic graphene analogs and their composites for Lithium ion batteries, Graphene, inorganic graphene analogs and their composites for lithium ion batteries, J. Mater. Chem. A **2** ,12104−12122 (2014).

[11] Hao J.Y., Zheng J.F., Ling F.L., Chen Y.K., Jing H. R., Zhou T.W., Fang L., Zhou M., Strain-engineered two-dimensional MoS 2 as anode material for performance enhancement of Li/Na-ion batteries, Sci . Rep. **8**, 2079 (2018).

[12] Li W., Yang Y.M., Gang Z., Zhang Y.W., Ultrafast and directional diffusion of lithium in phosphorene for high-performance lithium-ion battery, Nano Lett. **15**, 1691−1697 (2015).

[13] Wang D.S., Gao Y., Liu Y.H., Jin D., Gogotsi Y., Meng X., Du F., Chen G., Wei Y.J., First-Principles Calculations of Ti2N and Ti2NT2 (T = O, F, OH) Monolayers as Potential Anode Materials for Lithium-Ion Batteries and Beyond, J. Phys. Chem. C **121**, 13025−13034 (2017).

[14] Kim S.K., Chang H., Kim C.M., Yoo H., Kim H., Jang H.D., Fabrication of ternary silicon-carbon nanotubes-graphene composites by Co-assembly in evaporating droplets for enhanced electrochemical energy storage, J. Alloys Compd. **751,** 43−48 (2018).

[15] Sakurai H., Daiko T., Hirao T., A synthesis of sumanene, a fullerene fragment, Science, **301**, 1878−1878 (2003).

[16] Barth W. E.; Lawton R. G., A Practical, Large Scale Synthesis of the Corannulene System, *J. Am. Chem. Soc.*. **88,** 380–381 (1966).

[17] Lawton, R. G.; Barth, W. E. J. Am. Chem. Soc.., Synthesis of corannulene, **93**, 1730–1745 (1971).

[18] (a) Vessally E., Gharibzadeh F., Edjlali L., Eshaghi M., Mohammadi R., A DFT study on sumanene, corannulene and nanosheet as the anodes in Li−ion Batteries, *Iran. J. Chem. Chem. Eng*. (2020), 10.30492/ijcce.2020.106867.3568; **(b) Moladoust R.,** Sensing performance of boron nitride nanosheets to a toxic gas cyanogen chloride: Computational exploring**,** Chem. Rev. Lett. 2019, 2, 151-156; (c) Majedi S., Ghafur Rauf H., Boustanbakhsh M., DFT study on sensing possibility of the pristine and Al- and Ga-embeded $B_{12}N_{12}$ nanostructures toward hydrazine and hydrogen peroxide and their analogues**,** Chem. Rev. Lett. 2019, 2, 176-186; (d) Majedi S, Behmagham F., Vakili M., Theoretical view on interaction between boron nitride nanostructures and some drugs, *J. Chem. Lett.*, 2020, **1,** 19-24.

[19] Chai J.−D., Head−Gordon M., Long-range corrected hybrid density functionals with damped atom–atom dispersion corrections, *Phys. Chem. Chem. Phys.*, 2008, **10**, 6615 (2008).

[20] Frisch M.J., et. al., Gaussian09 program, (Gaussian Inc.,WalNangford, CT, 2009).

[21] S.F. Boys, F. Bernardi, *Mol. Phys.*, The calculation of small molecular interactions by the differences of separate total energies. Some procedures with reduced errors, **19**, 553–561 (1970).

[22] N. O'Boyle, A. Tenderholt, K. Langner, A library for package-independent computational chemistry algorithms, *J. Comput. Chem.* **29**,839–845 (2018).

[23] Hidehiro S., Taro D., Hiroyuki S., Toru A., Toshikazu H., Structural elucidation of sumanene and generation of its benzylic anions, *J. Am. Chem. Soc.*, 127 , 11580 −11581, (2005).

[24] Scott, L. T.; Hashemi, M. M.; Bratcher, M. S., Corannulene bowl-to-bowl inversion is rapid at room temperature, J. Am. Chem. Soc. **114** (5) 1920–1921 (1992).

[25] Denis P. A., Iribarne F., Theoretical investigation on the interaction between beryllium, magnesium and calcium with benzene, coronene, cirumcoronene and graphene, *Chem. Phys. Lett.*, **573**, 15−18 (2013).

[26] Gao Z., Chin C. S., Chiew J. H. K., Zhang J.J.C., A DFT study on nanocones, nanotubes (4, 0), nanosheets and fullerene C 60 as anodes in Mg-ion batteries, Energy, **10**, 1503 (2017).

HOW TO CITE THIS ARTICLE

Fatemeh Mohammad Alipour, Mirzaagha Babazadeh, Esmail Vessally, Akram Hosseinian, Parvaneh Dalir Kheirollahi Nezhad, "**Theoretical study of some graphene-Like nanoparticles as the anodes in K−ion Batteries**" International Journal of New Chemistry., 2023; 10(3), 197-212. DOI: 10.22034/ijnc.2022.552410.1295